

1 **Evidence for an unidentified non-photochemical ground-level**  
2 **source of formaldehyde in the Po Valley with potential**  
3 **implications for ozone production**

4  
5 **J. Kaiser<sup>1</sup>, G. M. Wolfe<sup>1,\*</sup>, B. Bohn<sup>2</sup>, S. Broch<sup>2</sup>, H. Fuchs<sup>2</sup>, L. N. Ganzeveld<sup>3</sup>, S.**  
6 **Gomm<sup>2</sup>, R. Häsel<sup>2</sup>, A. Hofzumahaus<sup>2</sup>, F. Holland<sup>2</sup>, J. Jäger<sup>2</sup>, X. Li<sup>2</sup>, I. Lohse<sup>2</sup>, K.**  
7 **Lu<sup>2,\*\*</sup>, A. S. H. Prévôt<sup>4</sup>, F. Rohrer<sup>2</sup>, R. Wegener<sup>2</sup>, R. Wolf<sup>4</sup>, T. F. Mentel<sup>2</sup>, A. Kiendler-**  
8 **Scharr<sup>2</sup>, A. Wahner<sup>2</sup>, and F. N. Keutsch<sup>1</sup>**

9 <sup>1</sup>Chemistry, University of Wisconsin-Madison, Madison, WI

10 <sup>2</sup>Institut für Energie- und Klimaforschung Troposphäre IEK-8, Forschungszentrum Jülich  
11 GmbH, Jülich, Germany

12 <sup>3</sup>Earth System Science and Climate Change, Wageningen University and Research Center,  
13 Wageningen, Netherlands

14 <sup>4</sup>Laboratory of Atmospheric Chemistry, Paul Scherrer Institute, Villigen, Switzerland

15 \*now at Joint Center for Earth Systems Technology, University of Maryland Baltimore County,  
16 Baltimore, MD, and at Atmospheric Chemistry and Dynamics Laboratory, NASA Goddard  
17 Space Flight Center, Greenbelt, MD

18 \*\*now at College of Environmental Sciences & Engineering, Peking University, Beijing, China

19 Correspondence to: F. N. Keutsch (keutsch@chem.wisc.edu)

20  
21 **Abstract**

22 Ozone concentrations in the Po Valley of Northern Italy often exceed international regulations.  
23 As both a source of radicals and an intermediate in the oxidation of most volatile organic  
24 compounds (VOCs), formaldehyde (HCHO) is a useful tracer for the oxidative processing of  
25 hydrocarbons that leads to ozone production. We investigate the sources of HCHO in the Po  
26 Valley using vertical profile measurements acquired from the airship Zeppelin NT over an

1 agricultural region during the PEGASOS 2012 campaign. Using a 1-D model, the total VOC  
2 oxidation rate is examined and discussed in the context of formaldehyde and ozone production in  
3 the early morning. While model and measurement discrepancies in OH reactivity are small (on  
4 average  $3.4\% \pm 13\%$ ), HCHO concentrations are underestimated by as much as 1.5 ppb (45%) in  
5 the convective mixed layer. A similar underestimate in HCHO was seen in the 2002-2003  
6 FORMAT Po-Valley measurements, though the additional source of HCHO was not identified.  
7 Oxidation of unmeasured VOC precursors cannot explain the missing HCHO source, as  
8 measured OH reactivity is explained by measured VOCs and their calculated oxidation products.  
9 We conclude that local direct emissions from agricultural land are the most likely source of  
10 missing HCHO. Model calculations demonstrate that radicals from degradation of this non-  
11 photochemical HCHO source increase model ozone production rates by as much as 0.6 ppb/hr  
12 (12%) before noon.

13

## 14 **1 Introduction**

15 Stagnant air masses, abundant solar radiation, and high anthropogenic emissions make Northern  
16 Italy's Po Valley one of Europe's most polluted regions. Previous measurements have shown  
17 that the regional O<sub>3</sub> background can reach as high as 90 ppb (Liu et al., 2007). Photochemical  
18 ozone production is tied to the reactions of NO<sub>x</sub> (NO+NO<sub>2</sub>), HO<sub>x</sub> (OH+HO<sub>2</sub>), and volatile  
19 organic compounds (VOCs). In the troposphere, NO<sub>2</sub> photodissociates to form oxygen atoms  
20 (R1), which then react with molecular oxygen to generate O<sub>3</sub> (R2). The partitioning of NO<sub>x</sub>  
21 between NO and NO<sub>2</sub> determines the production rate of O<sub>3</sub>. The hydroxyl-radical (OH) initiated  
22 oxidation of VOCs creates peroxy radicals (XO<sub>2</sub> = HO<sub>2</sub> + RO<sub>2</sub>) (R3). These radicals shift the  
23 partitioning of NO<sub>x</sub> radicals towards NO<sub>2</sub> (R4), thus increasing the net ozone production rate.



28 In this analysis, we define the net ozone production rate (P(O<sub>3</sub>)) as the calculated difference  
29 between the NO<sub>2</sub> photolysis rate (R1) and the rate of NO to NO<sub>2</sub> conversion by O<sub>3</sub>.

1 While measuring all VOCs and their oxidation products is non-trivial, formaldehyde (HCHO) is  
2 formed in the oxidation of nearly every VOC and thus provides a downstream constraint on this  
3 chemistry. In addition, photolysis of HCHO constitutes an important source of HO<sub>2</sub> radicals  
4 without consuming OH, effectively accelerating O<sub>3</sub> production via (R4) followed by (R1) and  
5 (R2).

6 In 2002-2003, the FORMAT (FORMaldehyde as A Tracer of oxidation in the troposphere)  
7 campaign aimed to use HCHO to trace the effect of VOC oxidation on ozone production in the  
8 Po Valley. Though modeling efforts focused primarily on the Milan urban plume, an agricultural  
9 region upwind of the city was also investigated in the 2003 FORMAT study (Liu et al., 2007).  
10 There, HCHO mixing ratios were up to two times higher than those predicted by regional  
11 chemistry transport models. Primary emissions were estimated to be a minor source of HCHO in  
12 the agricultural region (~10%), and OH-initiated oxidation of underrepresented local biogenic or  
13 anthropogenic VOC emissions was cited as the likely cause of underpredicted HCHO. Because  
14 the morning increase in HCHO was not well represented, and because the regional background  
15 was not well understood, the effect of anthropogenic emissions on the diurnal cycle under  
16 polluted conditions could not be reproduced by the model (Junkermann, 2009).

17 While HCHO measurements provide a product-based view of VOC oxidation, direct  
18 measurements of OH reactivity, the inverse lifetime of OH, can provide further insight into the  
19 instantaneous VOC oxidation rate. OH reactivity is calculated as

$$20 \quad OH \text{ reactivity } (s^{-1}) = \sum_i k_{X_i+OH} [X_i] \quad (1)$$

21 where  $k_{X_i+OH}$  are the rate coefficients for the reaction of all species X with OH. Field  
22 measurements of OH reactivity have been available since 2001, and Edwards et al. (2013) and  
23 Lou et al. (2010) provide summaries of recent comparisons of modeled and measured reactivity  
24 in a variety of environments. Notably, measurements in Paris demonstrated that more than half  
25 of the measured reactivity in highly aged continental air masses could not be explained by  
26 available measurements (Dolgorouky et al., 2012). The authors concluded the missing OH sink  
27 was likely (multi)oxidized compounds from processed anthropogenic emissions. Previous work  
28 has examined the effect of discrepancies between modeled and measured OH reactivity on  
29 calculated O<sub>3</sub> production potentials (Sadanaga et al., 2005; Yoshino et al., 2012). In one study in

1 Tokyo, including unmeasured VOC precursors indicated by OH reactivity measurements  
2 increased the calculated ozone production potential by as much as 8 ppb/hr (55%) (Yoshino et  
3 al., 2012).

4 Measurements of OH reactivity provide an upper bound on total VOC oxidation, and in  
5 conjunction with measurements of OH concentration, the total RO<sub>2</sub> production rate. Similarly, as  
6 HCHO is a major source of HO<sub>2</sub>, measurements of HCHO place a lower bound on calculated  
7 HO<sub>2</sub> production rates. Correcting for any missing OH reactivity or missing HCHO can increase  
8 model XO<sub>2</sub> production rates, in turn increasing P(O<sub>3</sub>).

9 Here, we provide an analysis of HCHO, OH reactivity, and O<sub>3</sub> production using an extensive set  
10 of measurements acquired onboard a Zeppelin airship during the Pan-European Gas-AeroSOls  
11 Climate Interaction Study (PEGASOS) in the Po-Valley region. Through the Zeppelin's slow  
12 flight speed, highly spatially and temporally resolved trace gas measurements were acquired (Li  
13 et al., 2014). The Zeppelin's unique flight abilities enabled vertical profiling flight tracks from as  
14 low as 50 m up to an altitude of ~750 m, making possible assessment of the role of exchange  
15 between the nocturnal boundary layer, residual layer, and growing mixed layer. In this study we  
16 focus the analysis on one flight for which a clear delineation between those layers occurred (Li et  
17 al., 2014). Using a 1-D chemical transport model, we examine the structure and chemical  
18 evolution of HCHO vertical profiles. By combining measurements of OH reactivity and VOC  
19 precursors, we investigate sources of HCHO in the agricultural regions of the Po-Valley. Finally,  
20 we discuss the effects of HCHO sources on calculated ozone production rates as a function of  
21 time and altitude.

22

## 23 **2 Methods**

### 24 **2.1 Zeppelin NT payload and July 12<sup>th</sup> flight**

25 The Zeppelin NT platform, its scientific payload, and the July 12<sup>th</sup> flight have been described  
26 previously (Li et al., 2014) and are described briefly here. Between 05:30 L.T. (Local Time =  
27 UTC + 2 h) and 10:45 L.T., the airship performed a series of near-surface vertical spirals starting  
28 at 50 m and reaching ~750 m above sea level (Fig. 1). The airship spiraled upward for ~15 min  
29 and then returned to lower altitudes within 5 min. The spirals were performed near a ground-

1 based field site at San Pietro Capofiume (SPC, 44°41'N, 11°38'E), which is a background urban  
2 site according to the European Monitoring and Evaluation Programme (EMEP) criteria  
3 (<http://www.nilu.no/projects/ccc/manual/>). The nearest urban areas include Bologna 25 km to the  
4 southwest and Ferrara 20 km to the north. The more immediate region consists primarily of  
5 wheat and corn fields which experienced intense harvesting activities during the campaign.

6 The instrumentation, time resolution, accuracy, and precision of the measurements are fully  
7 described in Li et al. (2014) and are summarized here (Table 1). Specifically, HCHO was  
8 measured at the Zeppelin nose boom using Fiber Laser-Induced Fluorescence (FILIF) (Hottle et  
9 al., 2009; DiGangi et al., 2011; Kaiser et al., 2014). The time resolution, precision, and accuracy  
10 of the measurement are 1 s, 20 – 200 ppt, and 15%, respectively. The  $2\sigma$  detection limit is 40 ppt.  
11 OH reactivity was measured from a platform on top of the Zeppelin by flash photolysis of ozone  
12 combined with time resolved OH detection in a flow tube. The instrument is an improved, more  
13 compact version of the instrument described by Lou et al. (2010). The accuracy of the OH  
14 reactivity data is 10%, with  $\pm 0.5 \text{ s}^{-1}$  systematic error of the zero-air decay rate coefficients  
15 (Gomm, 2014). Speciated C4-C11 VOCs, acetonitrile, and select oxygenated VOCs were  
16 measured by a fast gas chromatograph / mass spectrometer system with a time resolution of 180  
17 s and  $1 \sigma$  precision between 3% and 10% (Jäger, 2014). In addition, OH, HO<sub>2</sub>, NO, NO<sub>2</sub>, O<sub>3</sub>,  
18 CO, HONO, particle concentration/size distribution, solar actinic flux densities, temperature,  
19 pressure, relative humidity, and 3-D wind were measured simultaneously.

## 20 **2.2 Model simulations**

21 The Chemistry of Atmosphere-Forest Exchange (CAFE) model is a 1-D chemical transport  
22 model which has previously been used in steady-state analysis of trace gas fluxes above a pine  
23 forest (Wolfe and Thornton, 2011; Wolfe et al., 2011). For this study, the CAFE framework has  
24 been adapted to run in a time-dependent manner, and as the region is not forested, no canopy  
25 structure is included. The chemical mechanism generated by the Master Chemical Mechanism  
26 (MCM) v3.2 (Jenkin et al., 1997; Saunders et al., 2003; Bloss et al., 2005) contains near-explicit  
27 degradation schemes for all constrained VOCs as well as all relevant inorganic chemistry (more  
28 information available at <http://mcm.leeds.ac.uk/MCM>). The model was run with 7 evenly spaced  
29 altitude bins, with altitudes from 50-150 m for the lowest box and 650-750 m for the highest box.  
30 Measurements acquired during Zeppelin ascents were averaged into these 100 m altitude bins.

1 Because descents were performed much more quickly than ascents, data acquired during the  
2 ascents have higher spatial resolution than descent data. Where instrument time resolution limits  
3 data availability, concentrations are interpolated from data at surrounding altitude and time bins.  
4 In all model scenarios, measured photolysis frequencies are used where available. Otherwise,  
5 MCM calculated values are scaled according to the ratio of the calculated and measured  
6 photolysis rate of  $\text{NO}_2$ .

7 While methane was not measured at the SPC groundsite or from the Zeppelin, measurements of  
8  $\text{CH}_4$  were acquired from a mobile aerosol and trace gas laboratory ("Measurements Of Spatial  
9 QUantitative Immissions of Trace gases and Aerosols": MOSQUITA; Bukowiecki et al., 2002;  
10 Mohr et al., 2011), which was equipped with a Picarro Cavity Ring-Down Spectroscopy analyzer  
11 (Model G2401). MOSQUITA-based  $\text{CH}_4$  measurements were acquired from 8 June 2012 to 9  
12 July 2012. Though measurements are not available for the day of the flight studied here, the  
13 average concentration in the flight region of the Zeppelin (2355 ppb) is applied to this study.

14 In the base case scenario, the model is constrained to all measurements with the exception of  
15 HCHO. Given the extensive constraints, deposition, emission, and advection are not treated  
16 explicitly. Because deposition can be a non-negligible sink for many oxidized species (including  
17 HCHO), model results represent an upper limit on calculated mixing ratios. Turbulent diffusion  
18 is represented using K-theory, where diffusion coefficients are calculated using the Single  
19 Column chemistry and climate Model ECHAM4(SCM) (Ganzeveld et al., 2002). Further  
20 discussion of the eddy diffusion coefficient, uncertainty associated with turbulent diffusion, and  
21 the potential influence of deposition is available in the supplemental information.

22 To initialize non-measured species (e.g. speciated  $\text{RO}_2$  and organic nitrates), a "spin-up" 0-D  
23 diurnal model run was performed constraining all species to a combination of the lowest altitude  
24 Zeppelin measurements and available measurements from the nearby SPC ground site acquired  
25 between June 12<sup>th</sup> to July 10<sup>th</sup> 2012. This includes average diurnal profiles of  $\text{CO}$ ,  $\text{O}_3$ , benzene,  
26 toluene,  $\text{NO}_x$ , and relevant meteorological parameters. An average methane concentration of  
27 2355 ppb from the MOSQUITA mobile laboratory was assumed. Anthropogenic VOCs were  
28 scaled to ground benzene measurements according their observed relationship with benzene  
29 measurements acquired on the Zeppelin. To mimic the temperature dependence of isoprene  
30 emission rates, isoprene mixing ratios were assumed to be proportional to the cosine of the solar

1 zenith angle and scaled to available Zeppelin measurements. As isoprene concentrations are  
2 small ( $< 100$  ppt), the diurnal cycle has a negligible impact on modeled results. For 1-D model  
3 simulations, non-measured species are initialized to the output of the spin-up model at 06:00 L.T.  
4 on the 4<sup>th</sup> day scaled to HCHO measured on the Zeppelin as a function of altitude.

5

### 6 **3 Results and Discussion**

#### 7 **3.1 Observed HCHO and OH reactivity**

8 In the following section, we present observations of HCHO, VOCs, and OH reactivity acquired  
9 on the July 12<sup>th</sup> flight in the context of previous Po Valley measurements. A detailed  
10 presentation of additional trace gas measurements (notably HONO, NO<sub>x</sub>, O<sub>3</sub>, HO<sub>2</sub>, and H<sub>2</sub>O) as  
11 well as discussion of the delineation between residual layer, nocturnal boundary layer, and mixed  
12 layer can be found in Li et al. (2014).

13 Figure 2 shows measured HCHO, OH reactivity, and selected VOCs as a function of time and  
14 altitude. Primary biogenic VOC concentrations were low throughout the entire flight (isoprene  $<$   
15 60 ppt), which is consistent with previous measurements at Verzago, an agriculture site  
16 downwind of Milan (Steinbacher et al., 2005a). Anthropogenic VOCs such as toluene and  
17 benzene were around an order of magnitude lower than at Verzago in 2003 (Steinbacher et al.,  
18 2005b). In contrast to primary biogenic and anthropogenic VOCs, oxidized VOCs were abundant  
19 (reaching HCHO  $> 3.8$  ppb, acetaldehyde  $> 1.0$  ppb). The overall magnitude and morning rise of  
20 HCHO observed were similar to those observed previously in Spessa in 2002 (Junkermann,  
21 2009).

22 Before sunrise, elevated levels of toluene and other anthropogenic VOCs were observed in the  
23 residual layer compared to lower altitudes. Accumulation of VOC oxidation products including  
24 HCHO, methacrolein, and acetaldehyde was observed in the nocturnal boundary and in the  
25 residual layer. These oxidation products are either built up overnight or remain elevated from the  
26 previous day. After sunrise (05:45 L.T.), both biogenic and anthropogenic primary VOC increase  
27 in the developing mixed layer. The observed increase in HCHO mixing ratios lags that of  
28 primary VOCs, so that higher HCHO concentrations were observed  $\sim 4$  hrs after sunrise. The  
29 general vertical structure of the observed OH reactivity tracks well with HCHO, with elevated

1 values in nocturnal boundary and growing mixed layers. Based on the vertical structure of the  
2 observed HCHO and other trace gasses, potential sources of HCHO are discussed further in  
3 section 3.3.

### 4 **3.2 Base scenario modelled OH reactivity and HCHO**

5 The top panel of Fig. 3 shows the measured and modeled OH reactivity as a function of time and  
6 altitude. Overall, the magnitude and vertical structure is well captured by measured VOCs and  
7 their oxidation products. Where underestimated, the average discrepancy is less than 7%, with  
8 larger discrepancies at lower altitudes. Speciated model contributions to OH reactivity are shown  
9 in Fig. 4, calculated with all species (including HCHO) constrained to observations. NO<sub>x</sub>  
10 strongly influences the modeled OH reactivity, contributing 40% to modeled reactivity at 100 m,  
11 8:45 L.T. The contribution of measured VOCs and OVOCs is most significant in the mixed layer  
12 (26% at 100 m, 8:45 L.T.). Of all VOCs and OVOCs, HCHO consistently contributes the largest  
13 portion of calculated OH reactivity (HCHO reactivity  $\sim 0.2 \text{ s}^{-1} \text{ ppb}^{-1}$ , 8% of total modeled  
14 reactivity at 100 m and 8:45 L.T.).

15 Figure 3 also shows measured and modeled HCHO. Before 09:00 L.T., base case modeled  
16 HCHO matches measurements quite well. This is expected, as the model is initialized to  
17 measured HCHO mixing ratios, and low OH concentrations as well as lack of photolysis lead to  
18 very little change. Model/measurement discrepancy grows with time and is largest at low  
19 altitudes. Between 06:32 L.T. and 10:06 L.T., HCHO increases by as much as 1.3 ppb, while the  
20 model predicts no net increase. HCHO loss terms are unlikely to be overestimated as they are  
21 constrained by measured OH and measured HCHO photolysis frequencies, and could potentially  
22 be underestimated by neglecting deposition (see supplement). This finding implies that the  
23 model is missing either chemical HCHO production, advection of HCHO, or a local source of  
24 direct HCHO emissions.

### 25 **3.3 Potential sources of HCHO**

26 The oxidation of additional non-measured VOCs is often cited as a possible source of missing  
27 HCHO production in models (compared to FORMAT study, Junkermann, 2009). Using OH  
28 reactivity measurements, one can place an upper bound on the overall VOC oxidation rate in the  
29 atmosphere. As discussed above, measured VOCs and their modeled oxidation products explain



1 the majority of observed OH reactivity, though a small discrepancy is occasionally observed. To  
2 investigate the possibility of non-measured HCHO precursors, an additional model scenario is  
3 constructed in which the missing OH reactivity is assumed to be comprised entirely of ethene  
4 ( $C_2H_4$ ).  $C_2H_4$  was chosen as a surrogate species because it produces HCHO from OH and  $O_3$   
5 oxidation with respective yields of 160% (Niki et al., 1981) and 154% (Alam et al., 2011). Thus,  
6 the increase in modeled HCHO per increase in calculated OH reactivity is maximized.

7 Figure 3 shows the effect of increasing  $C_2H_4$  on HCHO and OH reactivity. While measured  
8 mixed-layer HCHO increases by as much as 1.3 ppb between 6:30 and 10:00 L.T., model HCHO  
9 increases by only 300 ppt. In order to generate the required HCHO, modeled  $C_2H_4$  would need to  
10 be increased such that calculated OH reactivity is up to 56% greater than the measurements.  
11 While the model vertical profile at 10:40 L.T. is in better agreement with measurements, at the  
12 09:24 L.T. vertical profile additional VOC precursors can explain no more than 0.26 ppb, or  
13 23%, of the missing HCHO budget. We therefore conclude that non-measured VOCs cannot  
14 explain the discrepancy in measured and modeled HCHO.

15 Another possible source of HCHO is transport from nearby urban centers. In the early morning,  
16 the average wind speed was less than 1.2 m/s, and the average HCHO lifetime was ~3.5 hr.  
17 Between 6:00 L.T. and 10:30 L.T., the bottom most layer in contact with the surface grows from  
18 less than 50 m to more than 600 m in height. Accounting for this dilution, and the HCHO  
19 lifetime and wind speed, and assuming a nighttime concentration in Bologna of 6 ppb (near the  
20 maximum nocturnal concentration reported in Milan (Junkermann, 2009)), the amount of HCHO  
21 advected could be no more than 90 ppt, or 7% of the missing HCHO budget. Additionally, no  
22 other long-lived tracers of anthropogenic influence (i.e. CO, xylenes) show a rise in the late  
23 morning. Finally, the vertical profile of the missing HCHO suggests a strong source near the  
24 ground which is convectively incorporated into the growing mixed layer. As advection of  
25 HCHO, e.g., from Bologna, would more likely affect the mixed layer as a whole, transport is an  
26 unlikely source of HCHO.

27 As the air aloft initially has slightly elevated levels of HCHO, entrainment of air from the  
28 residual layer into the mixed layer is an additional potential source of HCHO. Using  
29 ECHAM4(SCM) to investigate observations from the October 2005 field campaign over the  
30 Atlantic Ocean, French Guyana and Suriname, Ganzeveld et al. (2008) demonstrated the

1 assessment of daytime HCHO requires a thorough evaluation of the morning turbulent transport.  
2 The model predicted entrainment of HCHO would affect the daytime radical budget and  
3 resulting oxidative chemistry; however, limited observations in the residual layer did not allow  
4 for comparing SCM simulations with measurements. If entrainment was the primary cause of  
5 measurement and model discrepancy, the missing HCHO would be larger near the top of the  
6 boundary layer and when HCHO concentrations aloft are the highest. In this study, the largest  
7 discrepancies occur at the lowest altitudes and later in the morning. The highly resolved vertical  
8 measurements enabled by the Zeppelin aircraft demonstrate that for this study, entrainment is  
9 unlikely to be the primary cause of model/measurement discrepancies at low altitudes.

10 An additional potential source of HCHO is local direct emission from biomass burning or other  
11 anthropogenic activities. Aircraft measurements in 2003 showed evidence of biomass burning  
12 contribution to elevated HCHO in the agricultural regions of the Po Valley (Junkermann, 2009);  
13 however, these measurements were in September and October after the harvesting of the rice  
14 fields, and we did not see such strong local sources during the flight. Acetonitrile, a tracer of  
15 biomass burning, remains at a background levels of  $< 250$  ppt. As CO is a product of incomplete  
16 fuel combustion, it can be used to trace the influence of local traffic. CO does not increase  
17 significantly during the time HCHO increases in the mixed layer (Fig. 5). Using an emission  
18 ratio of 3.14 g HCHO/kg CO observed at a highway junction in Houston, Texas (Rappenglueck  
19 et al., 2013), the increase of 19 ppb in CO between 06:20 and 10:00 L.T., if wholly from traffic  
20 emissions, could account for only 57 ppt (4%) of the observed increase in HCHO. We therefore  
21 conclude neither biomass burning nor traffic can account for the relatively high levels of  
22 observed HCHO.

23 Finally, the soil, decaying plant matter from harvesting, or wheat or other crops in the region of  
24 the Zeppelin spirals may be a source of local direct HCHO emission. Measurements of  
25 oxygenated VOCs (OVOCs) from agricultural crops are limited. Konig et al. (1995) reported  
26 total OVOC emission rates from wheat were of  $10.9 \text{ ng g}^{-1} \text{ h}^{-1}$ , though speciated measurements  
27 of formaldehyde were not available. Dry weight HCHO emission rates from tree species in Italy  
28 are much higher, ranging from 382 to 590  $\text{ng g}^{-1} \text{ h}^{-1}$  (Kesselmeier et al., 1997). Oxygenated VOC  
29 emissions are expected to respond differently to light and temperature than terpenoids (Rinne et  
30 al., 2007), nevertheless the classic terpenoid exponential model is often extended to OVOC  
31 emissions. For example, for ground emissions of HCHO in a ponderosa pine forest, DiGangi et

1 al. (2011) applied an emission algorithm of  $E_{\text{HCHO}}=A \cdot \exp(\beta T)$ , where  $A=740 \text{ ng m}^{-2} \text{ h}^{-1}$  and  $\beta =$   
2  $0.07 \text{ }^\circ\text{C}^{-1}$ . The emissions were scaled by photosynthetically active radiation, with night time  
3 emissions fixed to 15% of daytime.

4 A final model scenario was constructed which incorporates direct emissions of HCHO according  
5 to the sunlight-weighted exponential emission function similar to DiGangi et al., employing a  
6 much smaller prefactor of  $A=375 \text{ ng m}^{-2} \text{ h}^{-1}$  to best capture the observed HCHO mixing ratios.  
7 These emissions are added as a direct HCHO source for the model's surface layer (0-50 m), with  
8 all other surface layer concentrations constrained to their lowest altitude measurement. The  
9 results are shown in Fig. 3. The vertical profile is mostly consistent with measurements, with  
10 possible discrepancies arising from uncertainty in eddy diffusion constants (see supplement).  
11 Due to the good agreement of this model result and the improbability of other HCHO sources,  
12 we conclude local direct emissions from agricultural land are the most likely source of additional  
13 HCHO.

14 The finding that direct biogenic emission could account for a large percentage of the observed  
15 increase in HCHO mixing ratio is in contrast with the Liu et al. (2007) assumption that direct  
16 emissions accounts for only ~10% of HCHO source in the agricultural Po Valley. Due to scarce  
17 data availability, limited information on chemical speciation, and only rough estimation of  
18 emission rates, models often assume a default emission rate for all oxygenated VOCs  
19 independent of land use or plant type (Karl et al., 2009). To realize the full potential of these  
20 oxidized VOCs as tracers of the photochemistry that forms secondary pollutants, and to  
21 understand their effects on such chemistry, thorough studies of direct emission are needed.

### 22 **3.4 Implications for ozone production**

23 An additional HCHO source, regardless of the type, will have a direct impact on calculated  
24 ozone production rates. The in-situ ozone production can be calculated as

$$25 \quad P(O_3) = k_{HO_2+NO}[HO_2][NO] + \sum_i k_{RO_2i+NO}[RO_{2i}][NO], \quad (2)$$

26 where  $NO_2$  is assumed to photodissociate leading to immediate ozone production (R1 and R2).  
27 In our MCM-based calculations, the formation of organic nitrates is accounted for in the  $RO_2 +$   
28  $NO$  reaction rates. As direct measurements of  $RO_2$  were not available on the Zeppelin, the

1 analysis presented here relies on speciated modeled RO<sub>2</sub> concentrations and reaction rates.  
2 Typical model RO<sub>2</sub> concentrations are between 10% and 30% of the sum of modeled RO<sub>2</sub> and  
3 measured HO<sub>2</sub>, such that HO<sub>2</sub> accounts for the majority of the modeled NO to NO<sub>2</sub> conversion.  
4 Because HCHO photolysis and oxidation accounts for as much as 39% model HO<sub>2</sub> production,  
5 failing to include all sources of HCHO has significant effects on calculated HO<sub>2</sub> concentrations.  
6 Though not probable in this analysis, if oxidation of unmeasured VOCs contributes significantly  
7 to the HCHO budget, RO<sub>2</sub> concentrations would likely be underestimated.

8 Because the effects of transport on O<sub>3</sub> may be large, we do not explicitly compare measured and  
9 modeled O<sub>3</sub> concentrations in this study. Instead, two model scenarios were constructed to  
10 estimate the impact of missing HCHO on HO<sub>2</sub> mixing ratios and therefore ozone production.  
11 Both simulations were carried out with HO<sub>2</sub> unconstrained, and HCHO was either fixed to  
12 observations or calculated by the model. Constraining HO<sub>2</sub> has a negligible effect on modeled  
13 HCHO concentrations. Because the difference in concentration of HO<sub>2</sub> between the two model  
14 scenarios is smaller than the measurement uncertainty (~12% compared to 30%), and because  
15 both model scenarios reproduce HO<sub>2</sub> concentration within the measurement uncertainty,  
16 measured and modeled HO<sub>2</sub> are not compared. At the observed mixed layer NO concentrations  
17 of ~1 ppb and an rate constant of  $k_{\text{HO}_2+\text{NO}} = 8.6 \cdot 10^{-12} \text{ cm}^3 \text{ molec}^{-1} \text{ s}^{-1}$ , an increase of just 1 ppt  
18 HO<sub>2</sub> corresponds to an additional 0.7 ppb/hr (14%) of ozone production. Figure 6 shows the  
19 difference in P(O<sub>3</sub>) driven by differences in calculated HO<sub>2</sub> concentrations. Assuming the trend  
20 in the discrepancy in HCHO continues to increase throughout the day, an increasing under-  
21 prediction of local ozone production rate is expected for this agricultural region.

22

#### 23 **4 Conclusions**

24 Using a near-explicit 1-D model and a comprehensive set of trace gas measurements acquired  
25 from a Zeppelin airship, we have examined VOC oxidation and its relationship to ozone  
26 production in the Po Valley. As in previous work in the region, our model was largely unable to  
27 reproduce the morning rise and high levels of observed HCHO. Measured OH reactivity,  
28 however, was explained by measured VOCs and their calculated oxidation products. The most  
29 probable source of missing HCHO is direct emission from the soil and plant matter beneath the  
30 Zeppelin. As a result of the underestimate in HCHO, model ozone production rates based on

1 HO<sub>2</sub> concentrations are underestimated by as much as 12% before noon, and the underestimate is  
2 expected to increase. When considering photochemical models of O<sub>3</sub> production, even small  
3 underestimates in HCHO can lead to large underestimates of local ozone production rates. For  
4 that reason, and considering the large portion of land used globally for similar agricultural  
5 purposes, direct measurements of OH reactivity and HCHO as well as improved OVOC emission  
6 inventories would aid in the prediction of high ozone events.

7

## 8 **Acknowledgements**

9 This work is within the PEGASOS project which is funded by the European Commission under  
10 the Framework Programme 7 (FP7-ENV-2010-265148). The authors would like to acknowledge  
11 all members of the PEGASOS flight and science teams. We also acknowledge Zeppelin  
12 Luftschifftechnik (ZLT) and Deutsche Zeppelin Reederei (DZR) for their cooperation. J. Jäger,  
13 R. Wegener, I. Lohse, and B. Bohn like to thank Deutsche Forschungsgemeinschaft for funding  
14 within the priority program HALO (WE-4384/2-2 and BO1580/4-1). J. Kaiser, G. M. Wolfe, and  
15 F. Keutsch like to thank Maria Cazorla for helping with the calibration of the HCHO  
16 measurements and NSF-AGS (1051338) and Forschungszentrum Jülich for support. G. Wolfe  
17 acknowledges support from the NOAA Climate and Global Change Postdoctoral Fellowship  
18 Program. J. Kaiser acknowledges support from the National Science Foundation Graduate  
19 Research Fellowship Program under Grant No. DGE-1256259. We would like to thank ARPA  
20 Emilia-Romagna (Region Agency for Environmental Protection in the Emilia-Romagna region  
21 Italy) and all participants in the Supersito Project for providing measurements at the SPC  
22 groundsite. The authors also acknowledge Christos Kaltsonoudis and Spyros Pandis from  
23 Laboratory of Air Quality Studies at the University of Patras for making CO data from the SPC  
24 ground site available.

25

## 26 **References**

27 Alam, M. S., Camredon, M., Rickard, A. R., Carr, T., Wyche, K. P., Hornsby, K. E., Monks, P.  
28 S., and Bloss, W. J.: Total radical yields from tropospheric ethene ozonolysis, *Phys. Chem.*  
29 *Chem. Phys.*, 13, 11002-11015, 10.1039/c0cp02342f, 2011.

1 Bloss, C., Wagner, V., Jenkin, M. E., Volkamer, R., Bloss, W. J., Lee, J. D., Heard, D. E., Wirtz,  
2 K., Martin-Reviejo, M., Rea, G., Wenger, J. C., and Pilling, M. J.: Development of a detailed  
3 chemical mechanism (MCMv3.1) for the atmospheric oxidation of aromatic hydrocarbons,  
4 *Atmos. Chem. Phys.*, 5, 641-664, doi:10.5194/acp-5-641-2005, 2005.

5 Bohn, B., Corlett, G. K., Gillmann, M., Sanghavi, S., Stange, G., Tensing, E., Vrekoussis, M.,  
6 Bloss, W. J., Clapp, L. J., Kortner, M., Dorn, H.-P., Monks, P. S., Platt, U., Plass-Dülmer, C., Mi-  
7 halopoulos, N., Heard, D. E., Clemitshaw, K. C., Meixner, F. X., Prevot, A. S. H., and Schmitt,  
8 R.: Photolysis frequency measurement techniques: results of a comparison within the ACCENT  
9 project, *Atmos. Chem. Phys.*, 8, 5373–5391, doi:10.5194/acp-8- 5373-2008, 2008.

10 Bukowiecki, N., Dommen, J., Prévôt, A. S. H., Richter, R., Weingartner, E., and Baltensperger,  
11 U.: A mobile pollutant measurement laboratory – measuring gas phase and aerosol ambient  
12 concentrations with high spatial and temporal resolution, *Atmos. Environ.*, 36, 5569–5579, doi:  
13 10.1016/S1352-2310(02)00694-5, 2002.

14 DiGangi, J., Boyle, E., Karl, T., Harley, P., Turnipseed, A., Kim, S., Cantrell, C., Maudlin, R.,  
15 Zheng, W., Flocke, F., Hall, S., Ullmann, K., Nakashima, Y., Paul, J., Wolfe, G., Desai, A.,  
16 Kajii, Y., Guenther, A., and Keutsch, F.: First direct measurements of formaldehyde flux via  
17 eddy covariance: implications for missing in-canopy formaldehyde sources, *Atmos. Chem.*  
18 *Phys.*, 11, 10565-10578, 10.5194/acp-11-10565-2011, 2011.

19 Dolgorouky, C., Gros, V., Sarda-Esteve, R., Sinha, V., Williams, J., Marchand, N., Sauvage, S.,  
20 Poulain, L., Sciare, J., and Bonsang, B.: Total OH reactivity measurements in Paris during the  
21 2010 MEGAPOLI winter campaign, *Atmos. Chem. Phys.*, 12, 9593-9612, 10.5194/acp-12-9593-  
22 2012, 2012.

23 Edwards, P., Evans, M., Furneaux, K., Hopkins, J., Ingham, T., Jones, C., Lee, J., Lewis, A.,  
24 Moller, S., Stone, D., Whalley, L., and Heard, D.: OH reactivity in a South East Asian tropical  
25 rainforest during the Oxidant and Particle Photochemical Processes (OP3) project, *Atmos. Chem.*  
26 *Phys.*, 13, 9497-9514, 10.5194/acp-13-9497-2013, 2013.

27 Fuchs, H., Bohn, B., Hofzumahaus, A., Holland, F., Lu, K., Nehr, S., Rohrer, F., and Wahner,  
28 A.: Detection of HO<sub>2</sub> by laser-induced fluorescence: calibration and interferences from RO<sub>2</sub>  
29 radicals, *Atmos. Meas. Techn.*, 4, 1209-1225, 10.5194/amt-4-1209-2011, 2011.

1 Ganzeveld, L., Lelieveld, J., Dentener, F., Krol, M., and Roelofs, G.: Atmosphere-biosphere  
2 trace gas exchanges simulated with a single-column model, *J. Geophys. Res.-Atmos.*, 107,  
3 10.1029/2001JD000684, 2002.

4 Ganzeveld, L., Eerdeken, G., Feig, G., Fischer, H., Harder, H., Konigstedt, R., Kubistin, D.,  
5 Martinez, M., Meixner, F., Scheeren, H., Sinha, V., Taraborrelli, D., Williams, J., de Arellano, J.,  
6 and Lelieveld, J.: Surface and boundary layer exchanges of volatile organic compounds, nitrogen  
7 oxides and ozone during the GABRIEL campaign, *Atmos. Chem. Phys.*, 8, 6223-6243,  
8 10.5194/acp-8-6223-2008, 2008.

9 Gerbig, C., Schmitgen, S., Kley, D., Volz-Thomas, A., Dewey, K., and Haaks, D.: An improved  
10 fast-response vacuum-UV resonance fluorescence CO instrument, *J. Geophys. Res.*, 104, 1699–  
11 1704, doi:10.1029/1998JD100031, 1999.

12 Gomm, S. : Luftgestützte Messung von HO<sub>x</sub>-Radikalkonzentrationen mittels Laser-induzierter  
13 Fluoreszenz auf einem Zeppelin NT: Untersuchung der atmosphärischen Oxidationsstärke der  
14 unteren Troposphäre, Ph. D., Bergische-Universität Wuppertal, 2014.

15 Holland, F., Hofzumahaus, A., Schäfer, R., Kraus, A., and Pätz, H. W.: Measurements of OH  
16 and HO<sub>2</sub> radical concentrations and photolysis frequencies during BERLIOZ, *J. Geophys. Res.-*  
17 *Atmos.*, 108, 10.1029/2001jd001393, 2003.

18 Hottle, J., Huisman, A., Digangi, J., Kammrath, A., Galloway, M., Coens, K., and Keutsch, F.: A  
19 Laser Induced Fluorescence-Based Instrument for In-Situ Measurements of Atmospheric  
20 Formaldehyde, *Environ. Sci. Technol.*, 43, 790-795, 10.1021/es801621f, 2009.

21 Jäger, J.: Airborne VOC measurements on board the Zeppelin NT during PEGASOS campaigns  
22 in 2012 deploying the improved Fast-GC-MSD System, Ph. D., Forschungszentrum Jülich  
23 GmbH, Jülich, Germany, 2014.

24 Jenkin, M., Saunders, S., and Pilling, M.: The tropospheric degradation of volatile organic  
25 compounds: A protocol for mechanism development, *Atmos. Environ.*, 31, 81-104,  
26 10.1016/S1352-2310(96)00105-7, 1997.

27 Junkermann, W.: On the distribution of formaldehyde in the western Po-Valley, Italy, during  
28 FORMAT 2002/2003, *Atmos. Chem. Phys.*, 9, 9187-9196, 2009.

1 Kaiser, J., Li, X., Tillmann, R., Acir, I., Holland, F., Rohrer, F., Wegener, R., and Keutsch, F. N.:  
2 Intercomparison of Hantzsch and fiber-laser-induced-fluorescence formaldehyde measurements,  
3 *Atmos. Meas. Tech.*, 7, 1571-1580, 10.5194/amt-7-1571-2014, 2014.

4 Karl, M., Guenther, A., Koble, R., Leip, A., and Seufert, G.: A new European plant-specific  
5 emission inventory of biogenic volatile organic compounds for use in atmospheric transport  
6 models, *Biogeosciences*, 6, 1059-1087, 2009.

7 Kesselmeier, J., Bode, K., Hofmann, U., Muller, H., Schafer, L., Wolf, A., Ciccioli, P.,  
8 Brancaleoni, E., Cecinato, A., Frattoni, M., Foster, P., Ferrari, C., Jacob, V., Fugit, J. L., Dutaur,  
9 L., Simon, V., and Torres, L.: Emission of short chained organic acids, aldehydes and  
10 monoterpenes from *Quercus ilex* L. and *Pinus pinea* L. in relation to physiological activities,  
11 carbon budget and emission algorithms, *Atmos. Environ.*, 31, 119-133, 10.1016/s1352-  
12 2310(97)00079-4, 1997.

13 Konig, G., Brunda, M., Puxbaum, H., Hewitt, C. N., Duckham, S. C., and Rudolph, J.: Relative  
14 contribution of oxygenated hydrocarbons to the total biogenic VOC emissions of selected Mid-  
15 European agricultural and natural plant-species, *Atmos. Environ.*, 29, 861-874, 10.1016/1352-  
16 2310(95)00026-u, 1995.

17 Li, X., Rohrer, F., Hofzumahaus, A., Brauers, T., Häsel, R., Bohn, B., Broch, S., Fuchs, H.,  
18 Gomm, S., Holland, F., Jäger, J., Kaiser, J., Keutsch, F. N., Lohse, I., Lu, K., Tillmann, R.,  
19 Wegener, R., Wolfe, G. M., Mentel, T. F., Kiendler-Scharr, A., and Wahner, A.: Missing Gas-  
20 Phase Source of HONO Inferred from Zeppelin Measurements in the Troposphere, *Science*, 344,  
21 292-296, 10.1126/science.1248999, 2014.

22 Liu, L., Andreani-Aksoyoglu, S., Keller, J., Ordonez, C., Junkermann, W., Hak, C., Braathen, G.,  
23 Reimann, S., Astorga-Llorens, C., Schultz, M., Prevot, A., and Isaksen, I.: A photochemical  
24 modeling study of ozone and formaldehyde generation and budget in the Po basin, *J. Geophys.*  
25 *Res.-Atmos.*, 112, 10.1029/2006JD008172, 2007.

26 Lou, S., Holland, F., Rohrer, F., Lu, K., Bohn, B., Brauers, T., Chang, C., Fuchs, H., Häsel, R.,  
27 Kita, K., Kondo, Y., Li, X., Shao, M., Zeng, L., Wahner, A., Zhang, Y., Wang, W., and  
28 Hofzumahaus, A.: Atmospheric OH reactivities in the Pearl River Delta – China in summer



1 2006: measurement and model results, *Atmos. Chem. Phys.*, 10, 11243–11260, doi:10.5194/acp-  
2 10-11243-2010, 2010.

3 Mohr, C., Richter, R., DeCarlo, P. F., Prévôt, A. S. H., and Baltensperger, U.: Spatial variation  
4 of chemical composition and sources of submicron aerosol in Zurich during wintertime using  
5 mobile aerosol mass spectrometer data, *Atmos. Chem. Phys.*, 11, 7465-7482, doi:10.5194/acp-  
6 11-7465-2011, 2011.

7 Niki, H., Maker, P. D., M., S. C., and Breitenbach, L. P.: An FTIR study of mechanisms for the  
8 HO radical initiated oxidation of C<sub>2</sub>H<sub>4</sub> in the presence of NO: Detection of glycolaldehyde,  
9 *Chem. Phys. Lett.*, 80, 499–503, 1981.

10 Rappenglueck, B., Lubertino, G., Alvarez, S., Golovko, J., Czader, B., and Ackermann, L.:  
11 Radical precursors and related species from traffic as observed and modeled at an urban highway  
12 junction, *JAPCA J. Air Waste Ma.*, 63, 1270-1286, 10.1080/10962247.2013.822438, 2013.

13 Rinne, J., Taipale, R., Markkanen, T., Ruuskanen, T. M., Hellen, H., Kajos, M. K., Vesala, T.,  
14 and Kulmala, M.: Hydrocarbon fluxes above a Scots pine forest canopy: measurements and  
15 modeling, *Atmos. Chem. Phys.*, 7, 3361-3372, 2007.

16 Sadanaga, Y., Yoshino, A., Kato, S., and Kajii, Y.: Measurements of OH reactivity and  
17 photochemical ozone production in the urban atmosphere, *Environ. Sci. Technol.*, 39, 8847-  
18 8852, 10.1021/es049457p, 2005.

19 Saunders, S., Jenkin, M., Derwent, R., and Pilling, M.: Protocol for the development of the  
20 Master Chemical Mechanism, MCM v3 (Part A): tropospheric degradation of non-aromatic  
21 volatile organic compounds, *Atmos. Chem. Phys.*, 3, 161-180, 2003.

22 Steinbacher, M., Dommen, J., Ordonez, C., Reimann, S., Gruebler, F., Staehelin, J., Andreani-  
23 Aksoyoglu, S., and Prevot, A. S. H.: Volatile organic compounds in the Po Basin. part B:  
24 Biogenic VOCs, *J. Atmos. Chem.*, 51, 293-315, 10.1007/s10874-005-3577-0, 2005a.

25 Steinbacher, M., Dommen, J., Ordonez, C., Reimann, S., Gruebler, F. C., Staehelin, J., and  
26 Prevot, A. S. H.: Volatile organic compounds in the Po Basin. part A: Anthropogenic VOCs, *J.*  
27 *Atmos. Chem.*, 51, 271-291, 10.1007/s10874-005-3576-1, 2005b.

1 Wolfe, G., and Thornton, J.: The Chemistry of Atmosphere-Forest Exchange (CAFE) Model -  
2 Part 1: Model description and characterization, *Atmos. Chem. Phys.*, 11, 77-101, 10.5194/acp-  
3 11-77-2011, 2011.

4 Wolfe, G., Thornton, J., Bouvier-Brown, N., Goldstein, A., Park, J., McKay, M., Matross, D.,  
5 Mao, J., Brune, W., LaFranchi, B., Browne, E., Min, K., Wooldridge, P., Cohen, R., Crouse, J.,  
6 Faloona, I., Gilman, J., Kuster, W., de Gouw, J., Huisman, A., and Keutsch, F.: The Chemistry  
7 of Atmosphere-Forest Exchange (CAFE) Model - Part 2: Application to BEARPEX-2007  
8 observations, *Atmos. Chem. Phys.*, 11, 1269-1294, 10.5194/acp-11-1269-2011, 2011.

9 Yoshino, A., Nakashima, Y., Miyazaki, K., Kato, S., Suthawaree, J., Shimo, N., Matsunaga, S.,  
10 Chatani, S., Apel, E., Greenberg, J., Guenther, A., Ueno, H., Sasaki, H., Hoshi, J., Yokota, H.,  
11 Ishii, K., and Kajii, Y.: Air quality diagnosis from comprehensive observations of total OH  
12 reactivity and reactive trace species in urban central Tokyo, *Atmos. Environ.*, 49, 51-59,  
13 10.1016/j.atmosenv.2011.12.029, 2012.

1 Table 1. Zeppelin-based measurements used for the analysis of O<sub>3</sub> and HCHO production

Parameter	Technique	Precision (1 $\sigma$ )	Accuracy
HCHO	FILIF <sup>a</sup>	20-200ppt/s	15%
HONO	LOPAP <sup>b</sup>	1.3 ppt/180 s	12%
OH	Laser induced fluorescence <sup>c</sup>	Day LOD: 1.3x 10 <sup>6</sup> cm <sup>-3</sup> /42 s Night LOD: 0.67x 10 <sup>6</sup> cm <sup>-3</sup> /42 s	14%
HO <sub>2</sub>	Laser induced fluorescence <sup>d</sup>	Day LOD: 81 x 10 <sup>6</sup> cm <sup>-3</sup> /42 s Night LOD: 36x 10 <sup>6</sup> cm <sup>-3</sup> /42 s	24-30%
OH reactivity	Laser induced fluorescence <sup>e</sup>	6%/2 min (standarddeviation)	10%
NO	Chemiluminescence <sup>f</sup>	10 ppt/60 s	5%
NO <sub>2</sub>	Conversion to NO <sup>g</sup> followed by chemiluminescence <sup>f</sup>	30 ppt/60 s	7.5%
O <sub>3</sub>	UV absorption <sup>h</sup>	1 ppb/20 s	3%
CO	Resonance fluorescence <sup>i</sup>	5 ppb/1 s	5%
VOCs	Fast GC/MS <sup>j</sup>	3-10%/180 s	15%
Photolysis frequencies	Spectroradiometer <sup>k</sup>	-- (1 s) <sup>k</sup>	15% <sup>k</sup>
Relative humidity	Vaisala HUMICAP HMP45	0.1% RH/1 s	2% RH
Temperature	PT100	0.1 °C/1 s	0.1 °C
Pressure	Barometric SETRA	<0.5 mbar/1 s	33 mbar

2 <sup>a</sup>Fiber laser-induced fluorescence (Hottle et al., 2009).

3 <sup>b</sup>Long path absorption photometry (Li et al., 2014).

4 <sup>c</sup>Holland et al., (2003).

5 <sup>d</sup>Fuchs et al., (2011).

6 <sup>e</sup>Lou et al., (2010).

7 <sup>f</sup>ECOPHYSICS (type TR780)

8 <sup>g</sup>Photolytic blue light converter (Droplet Technologies type BLC)

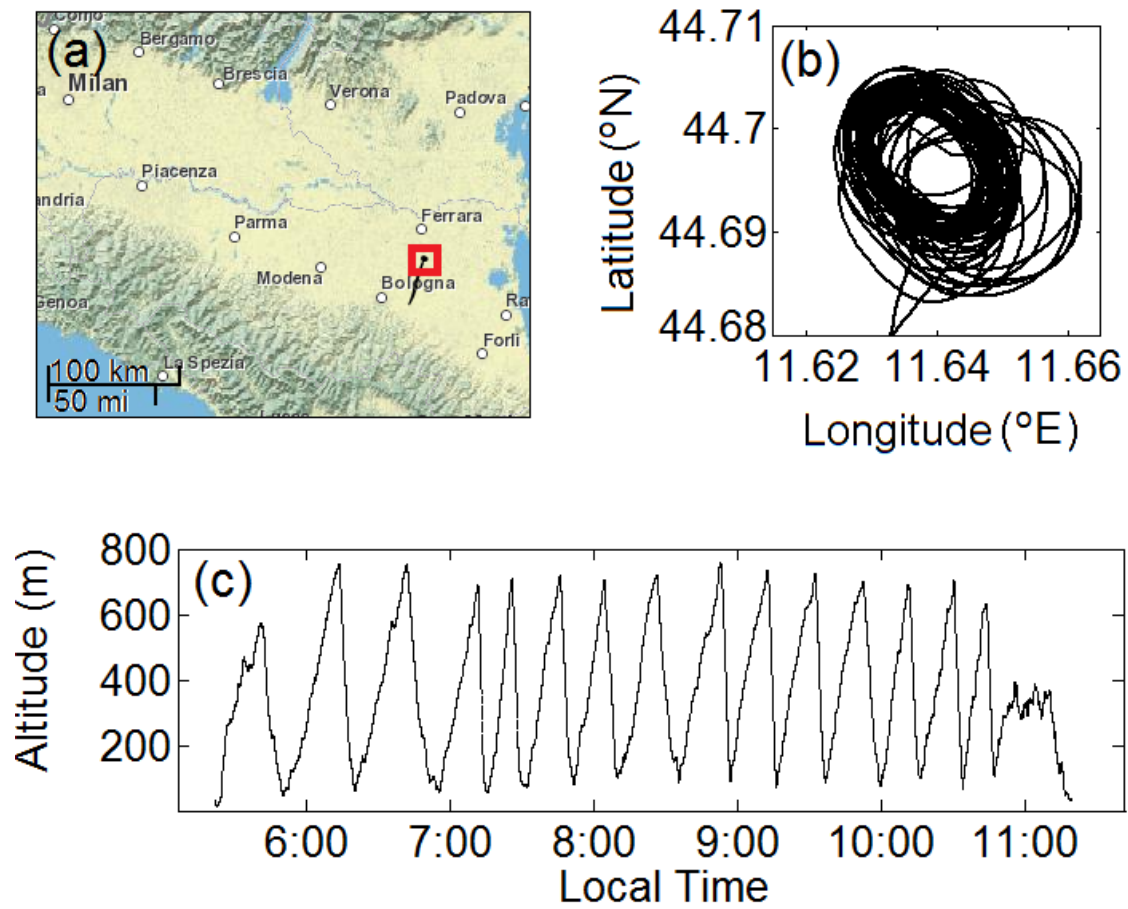
9 <sup>h</sup>ENVIRONNEMENT S. A. (type O342M)

10 <sup>i</sup>Gerbig et al., (1999).

11 <sup>j</sup>Gas chromatography/mass spectrometry (Jäger, 2014).

12 <sup>k</sup>Bohn et al. (2008). Accuracy and precision are dependent on conditions and photolysis process.

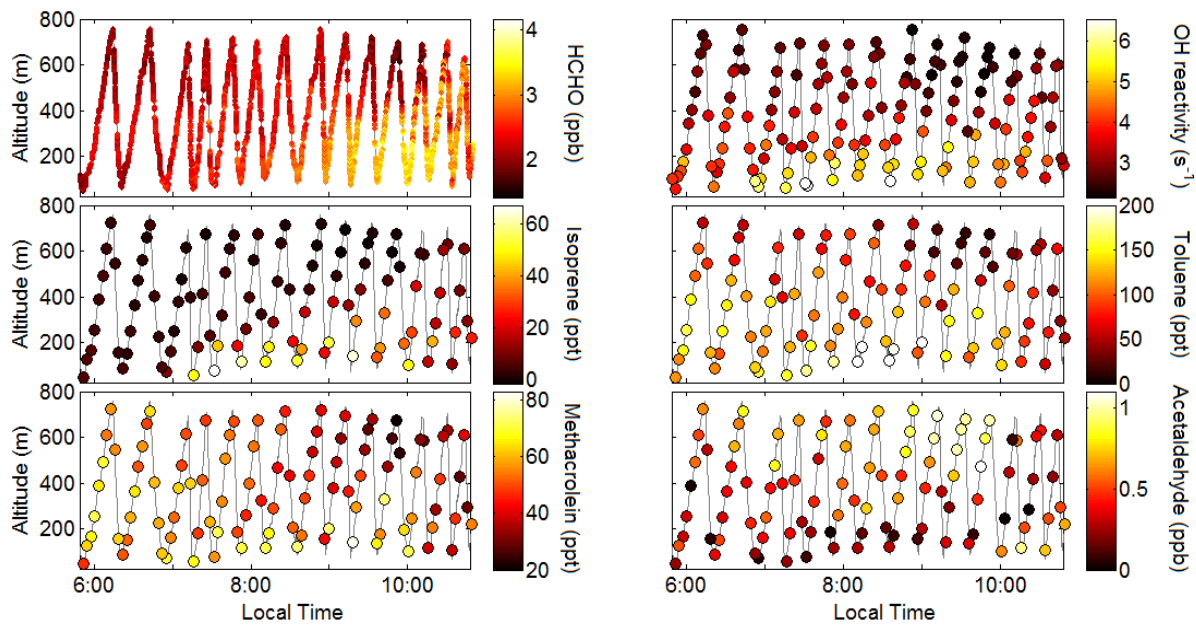
13 The 15% accuracy is a conservative estimate covering important photolysis frequencies.



1

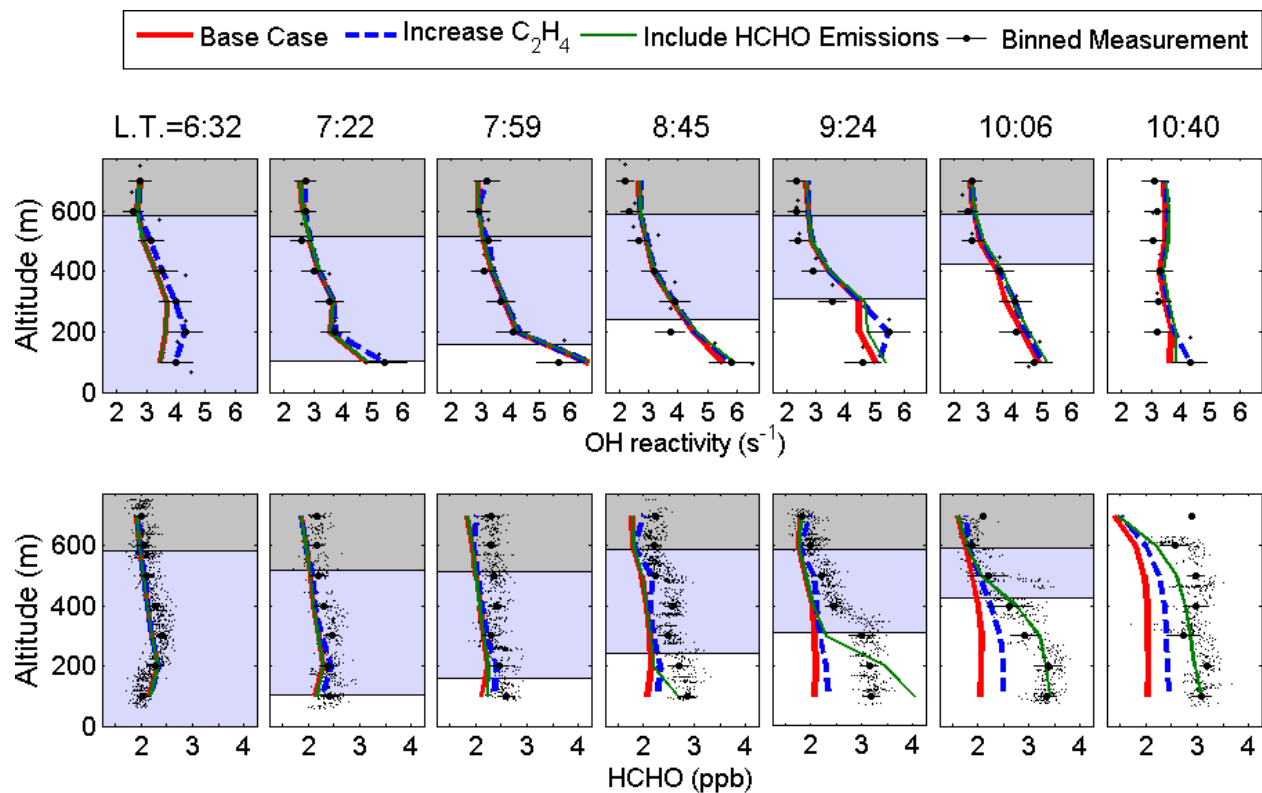
2 Figure 1. (a) Po Basin, with July 12, 2012 flight track shown in the box and enlarged in (b). (c)

3 Zeppelin altitude during flight.

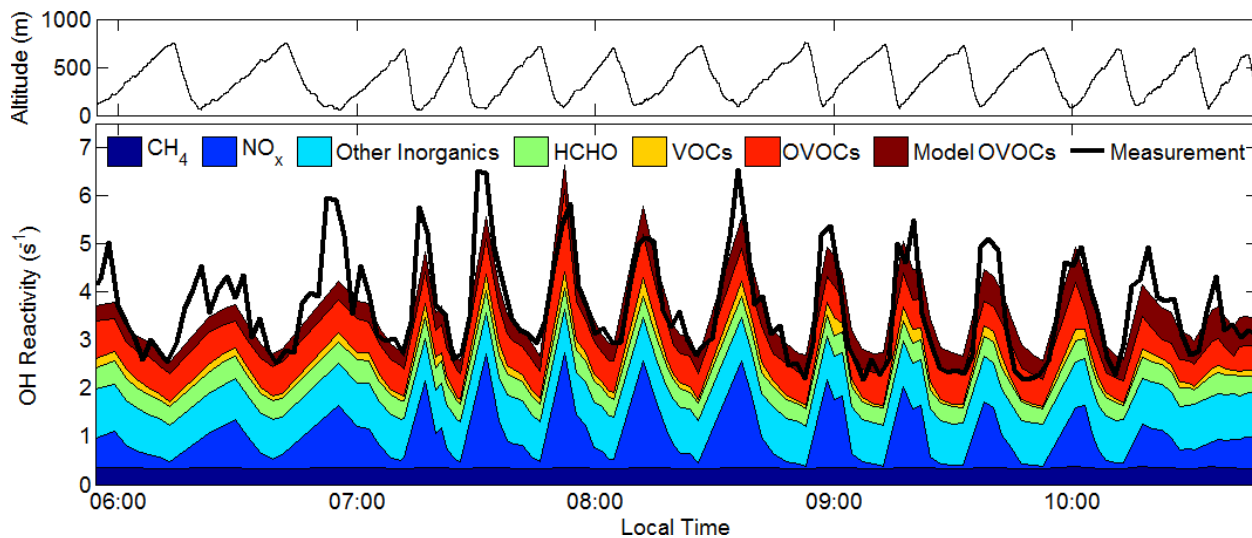


1

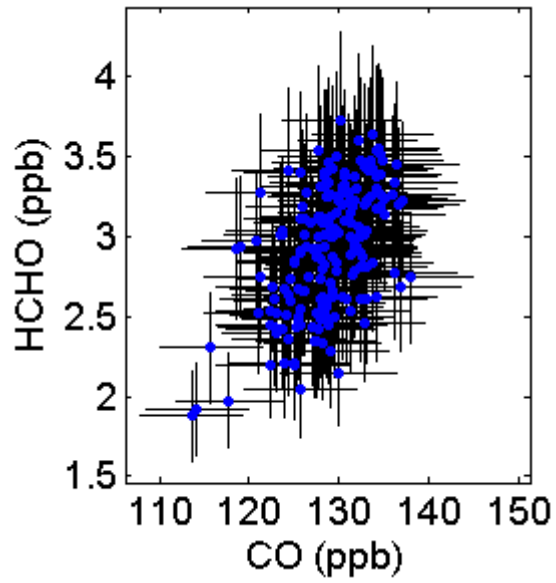
2 Figure 2. Flight pattern colored by selected measurements.



1  
 2 Figure 3. Measured and calculated OH reactivity and HCHO vertical profiles for every other  
 3 Zeppelin ascent. Error bars on OH reactivity represent the measurement precision. Error bars on  
 4 HCHO represent the standard deviation of the measurements in the given altitude bin. The gray,  
 5 blue, and white areas represent the residual layer, the nocturnal boundary layer, and the mixed  
 6 layer, respectively. Layer height was determined by the observed steep gradients in O<sub>3</sub> mixing  
 7 ratios, as detailed in Li et al. (2014). Model scenarios are described in more detail in sections 3.2  
 8 and 3.3.

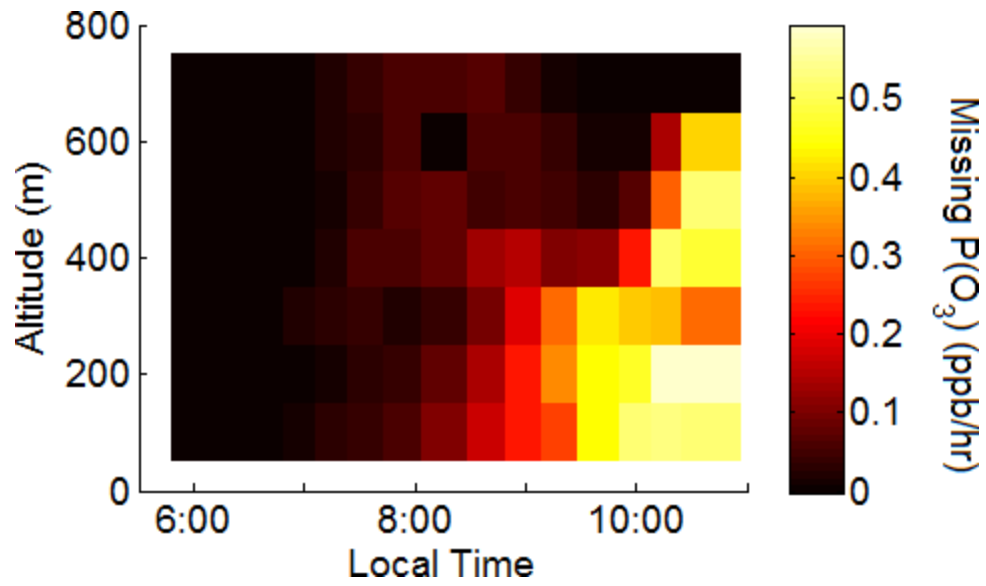


1  
 2 Figure 4. Contributions to calculated OH reactivity as a function of time. Only data acquired  
 3 during the ascents is used in the calculated reactivity. The VOC category consists of isoprene,  
 4 toluene, benzene, xylenes, ethylbenzene, C4-C9 straight chain alkanes, styrene,  
 5 trimethylbenzene, 1-pentene, cis-2-pentene, cyclohexanone, propylbenzene, isopropylbenzene,  
 6 isopentane, benzaldehyde, and 1-butene. The OVOC category consists of C2-C6 straight chain  
 7 aldehydes, acetone, methanol, ethanol, methyl acetate, ethyl acetate, methacrolein, methyl ethyl  
 8 ketone, methyl vinyl ketone, and 1-propanol. The inorganics category consists of CO, H<sub>2</sub>,  
 9 HONO, HO<sub>2</sub> and O<sub>3</sub>. Model OVOCs are non-measured oxidation products calculated by the  
 10 MCM.



- 1
- 2 Figure 5. HCHO and CO in the mixed layer. Error bars represent instrument accuracy. There is
- 3 little variation in mixed layer CO, and the correlation with HCHO is small ( $r^2 = 0.29$ ).





1  
 2 Figure 6. Underestimate in ozone production rate caused by the modeled underestimate in  
 3 HCHO as a function of time and altitude. Missing P(O<sub>3</sub>) is defined as P(O<sub>3</sub>) calculated using  
 4 measured HCHO minus P(O<sub>3</sub>) calculated using modeled HCHO.